Open Access Full Text Article

ORIGINAL RESEARCH

Molecular Subtypes Defined by Cuproptosis-Associated Genes, Prognostic Model Development, and Tumor Immune Microenvironment Characterization in Adrenocortical Carcinoma

Qi Huang [1–3],*, Xu-Yun Huang[1,2],*, Yu-Ting Xue[1,2],*, Xiao-Hui Wu[1,2],*, Yu-Peng Wu[1,2],*, Zhi-Bin Ke[1,2], Zhen Kang[1,2], Yi-Cheng Xu[1,2], Dong-Ning Chen[1,2], Yong Wei [1,2], Xue-Yi Xue [1,2], Zhi-Yang Huang[3], Ning Xu [1,2,4]

[1]Department of Urology, Urology Research Institute, the First Affiliated Hospital, Fujian Medical University, Fuzhou, 350005, People's Republic of China; [2]Department of Urology, National Regional Medical Center, Binhai Campus of the First Affiliated Hospital, Fujian Medical University, Fuzhou, 350212, People's Republic of China; [3]Department of Urology, Quanzhou First Hospital, Fujian Medical University, Quanzhou, 362000, People's Republic of China; [4]Fujian Key Laboratory of Precision Medicine for Cancer, the First Affiliated Hospital, Fujian Medical University, Fuzhou, 350005, People's Republic of China

*These authors contributed equally to this work

Correspondence: Ning Xu, Department of Urology, Urology Research Institute, the First Affiliated Hospital, Fujian Medical University, 20 Chazhong Road, Fuzhou, 350005, People's Republic of China, Tel +86-059187981687, Email drxun@fjmu.edu.cn; Zhi-Yang Huang, Department of Urology, Quanzhou First Hospital, Fujian Medical University, No. 250, East Street, Licheng District, Quanzhou, Fujian, 362000, People's Republic of China, Email hzy8902@126.com

Introduction: This study aims to explore the role of cuproptosis-related genes in ACC, utilizing data from TCGA and GEO repositories, and to develop a predictive model for patient stratification.

Methods: A cohort of 123 ACC patients with survival data was analyzed. RNA-seq data of 17 CRGs were examined, and univariate Cox regression identified prognostic CRGs. A cuproptosis-related network was constructed to show interactions between CRGs. Consensus clustering classified ACC into three subtypes, with transcriptional and survival differences assessed by PCA and survival analysis. Gene set variation analysis (GSVA) and ssGSEA evaluated functional and immune infiltration characteristics across subtypes. Differentially expressed genes (DEGs) were identified, and gene clusters were established. A risk score (CRG_score) was generated using LASSO and multivariate Cox regression, validated across datasets. Tumor microenvironment, stem cell index, mutation status, drug sensitivity, and hormone synthesis were examined in relation to the CRG_score. Protein expression of key genes was validated, and functional studies on ASF1B and NDRG4 were performed.

Results: Three ACC subtypes were identified with distinct survival outcomes. Subtype B showed the worst prognosis, while subtype C had the best. We identified 214 DEGs linked to cell proliferation and classified patients into three gene clusters, confirming their prognostic value. The CRG_score predicted patient outcomes, with high-risk patients demonstrating worse survival and possible resistance to immunotherapy. Drug sensitivity analysis suggested higher responsiveness to doxorubicin and etoposide in high-risk patients.

Conclusion: This study suggests the potential prognostic value of CRGs in ACC. The CRG_score model provides a robust tool for risk stratification, with implications for treatment strategies.

Keywords: cuproptosis, overall survival, immune microenvironment, molecular signature

Introduction

Adrenocortical carcinoma (ACC), an infrequent malignancy originating from adrenal cortical cells.[1] Despite radical surgical resection being the mainstay of potentially curative treatment for ACC, its efficacy diminishes with disease progression.[2] Regrettably, up to 70% of patients undergoing curative resection face disease recurrence, often accompanied by metastasis.[3] Clinical trials targeting ACC have largely failed to yield significant survival benefits or to capitalize on the potential of targeted and immunotherapies. In light of advancements in precision medicine, there is a pressing need to identify specific patient subgroups who may derive meaningful benefits from treatment interventions.

Copper (Cu) plays a critical role as a trace element, being indispensable for various biological processes in organisms, including cellular respiration and the regulation of oxidative stress.[4] In the adrenal gland, Cu is crucial for assisting norepinephrine production by facilitating its passage into the secretory pathway.[5] Recently, Tsvetkov et al[6] introduced the notion of cuproptosis, describing a mechanism in which copper induces cellular death by provoking protein toxic stress. FDX1 has emerged as a pivotal player in regulating cuproptosis, as evidenced by studies demonstrating that its absence confers cellular protection against this form of cell death.[7]

In this study, we utilized data from the TCGA and GEO repositories to classify ACC samples into three distinct categories based on cuproptosis-related gene (CRG) expression patterns. We identified prognostic genes associated with cuproptosis by overlapping differentially expressed genes (DEGs) linked to prognosis within these categories. These cuproptosis-related prognostic genes were further organized into three gene clusters according to their expression profiles. A predictive model was developed from this data, and we extensively evaluated the relationship between different risk categories and factors such as the tumor immune microenvironment (TIME), steroid secretion, and proliferation indicators. Initial experimental validation supported the biological relevance of two potential biomarkers in ACC. These findings suggest opportunities for improving ACC classification methods and advancing targeted therapeutic approaches.

Materials and Methods

Data Collection and Selection of CRGs

We obtained three datasets comprising RNA sequencing, gene chip data, and clinical information from the TCGA and GEO repositories, collectively encompassing 138 ACC samples (TCGA ACC, n=90; GSE19750, n=48). The clinical data encompassed a range of parameters, including age, gender, pathological grade, stage, and survival-related information. Tsvetkov et al[6] identified genes involved in the regulation of cuproptosis, including FDX1, LIAS, LIPT1, LIPT2, DLD, DLAT, PDHA1, PDHB, MTF1, GLS, and CDKN2A. Copper induces cell death by targeting lipoylated TCA cycle proteins, with DBT, GCSH, and DLST being critical enzymes in the protein lipoylation process.[6] SLC31A1, ATP7A, and ATP7B are involved in maintaining copper homeostasis, preventing excessive accumulation of copper ions within cells.[6] Activation of the NLRP3 inflammasome can inhibit copper-induced neuropathology.[8] Inhibition of NRF2 expression significantly promotes the accumulation of lipid peroxidation, increasing the sensitivity of HCC cells to Cu-induced cell death.[9] Therefore, we selected 19 CRGs (SLC31A1, ATP7A, ATP7B, FDX1, LIAS, LIPT1, LIPT2, DLD, DLAT, PDHA1, PDHB, MTF1, GLS, CDKN2A, DBT, GCSH, DLST, NLRP3, NRF2) for further study.

Mutations and CNVs of CRGs

Somatic mutations and CNVs were obtained from the TCGA database. Initially, we calculated the frequency of somatic mutations in the samples to identify CRGs with high mutation frequencies. Subsequently, we analyzed somatic CNVs of the CRGs and examined the correlation between CNVs and mRNA expression levels. Additionally, we determined the chromosomal locations of these CRGs.

CRGs-Based Consensus Clustering Analysis

Employing the R package "ConsensusClusterPlus" we amalgamated two datasets to execute unsupervised clustering analysis via consensus methodology. Based on their CRG expression profiles, patients were classified into distinct molecular subtypes. The clustering process followed specific criteria, aiming for a gradual and smooth increase in the

cumulative distribution function (CDF) curve, the absence of subgroups with small sample sizes, and an enhancement in within-group correlations alongside a reduction in between-group correlations. After consensus clustering, differences in CRG expression were assessed through Principal Component Analysis (PCA) using the "*ggplot2*" package in R. Additionally, we conducted Gene Set Variation Analysis (GSVA) to explore the differences in CRGs involved in various biological processes. This analysis utilized the hallmark gene set (*c2.cp.kegg.v7.2*), which was sourced from the MSigDB database.

Investigation into Clinicopathological Features, Prognosis, and Immune Cell Infiltration in ACC Subtypes

Through consensus clustering, we comprehensively analyzed the clinical significance of the three cuproptosis subtypes, investigating their correlations with molecular subtypes, clinicopathological characteristics, patterns of CRGs expression, and prognostic implications. Patient characteristics including stage, pathological grade, gender, and age were evaluated, with Kaplan-Meier curves utilized for overall survival (OS) comparison among the three subtypes. Additionally, we employed the single-sample Gene Set Enrichment Analysis (ssGSEA) algorithm to explore the correlation between the three subtypes and the infiltration of immune cells.

Analysis and Functional Interpretation of DEGs in Cuproptosis Patterns

DEGs were identified using the R package "limma" with significance determined at a threshold of p-value < 0.05 and a fold change $\geq$ 1.5. Following this, we performed GO and KEGG enrichment analyses with the R packages "clusterProfiler", "*enrichplot*" and "*ggplot2*" to explore the functional roles of the identified DEGs linked to cuproptosis patterns.

Development of the Prognostic CRG_score Associated with Cuproptosis

Our objective was to devise the Cuproptosis-related Prognostic CRG_score, which quantifies individual tumor cuproptosis patterns. Initially, a univariate Cox analysis pinpointed DEGs linked to ACC OS. Subsequently, unsupervised clustering stratified patients into three clusters (A, B, C) based on prognostic CRG expression. The dataset was randomly divided into training (n = 51) and validation (n = 50) sets, maintaining a 1:1 ratio. In the training cohort, the CRG_score was developed using LASSO analysis and multivariate Cox regression to select prognostic DEGs. This score was calculated using the formula: CRG_score = Σ(Expi * coefi), where coefi represents the risk coefficient and Expi denotes the expression level of the respective DEGs. Patients were categorized into low- and high-risk groups based on the median score, with the same methodology applied to the validation and entire cohorts. The predictive efficacy was assessed through survival analysis using Kaplan-Meier curves and ROC curve analysis.

Immunohistochemistry (IHC) Staining

In this study, we analyzed tissue samples from a total of ten cases, consisting of five adrenocortical adenomas and five ACC. These samples were obtained from patients who underwent urological surgery at the First Affiliated Hospital of Fujian Medical University. These samples were processed into 5μM thick sections and underwent antigen retrieval using citric acid buffer in boiling water for 20 minutes after dewaxing and hydration. Immunohistochemical staining was performed using the UltraSensitiveTM SP immunohistochemical kit (KIT-9710) from Maixin Biotechnologies, along with ASF1B (YT0369, Immunoway, 1/200) and NDRG4 (YT3006, Immunoway, 1/200) antibodies. We conducted semi-quantitative analysis of the staining results using ImageJ software to determine optical density (OD) values and positive area. Integrated optical density (IOD) was calculated, and the average optical density (AOD) was assessed as AOD = IOD / area to evaluate relative expression.[10]

Cell Line Origin and Culture Conditions

The SW-13 cell line, initially established by Leibovitz A in August 1971, was derived from a 55-year-old White female patient diagnosed with stage IV primary adrenocortical small cell carcinoma.[11] This epithelial-like cell line has since

been extensively utilized in studies related to adrenocortical carcinoma (ACC).[12,13] In our research, SW-13 cells were cultured using L15 supplemented with 10% fetal bovine serum and 1% penicillin-streptomycin. The cells were maintained in an incubator set at 37°C with 5% CO2. Once the cell density reached 70% to 80%, as observed under an inverted microscope, the cells were subjected to passaging using 0.25% trypsin for subsequent experiments.

Western Bolt
Protein concentrations were quantified using a BCA assay kit after preparing cell lysates with RIPA buffer. Subsequently, proteins underwent separation via SDS-PAGE and transfer onto PVDF membranes. Following blocking with NcmBlot blocking buffer, membranes were exposed to primary antibodies against β-Tubulin, β-actin, ASF1B, NDRG4, PDL-1 and VEGFA overnight at 4°C. Following rinsing, membranes underwent treatment with an HRP-conjugated secondary antibody and were subsequently visualized using ECL reagent.

qRT-PCR
Following culture in 6-well plates until reaching approximately 80% confluence, SW-13 cells were transfected with corresponding short hairpin RNAs (shRNAs) using Lipo8000^{TM} reagent (C0533, Beyotime), adhering to the manufacturer's instructions. After 48 hours of transfection, we assessed the expression levels of ASF1B and NDRG4 through qRT-PCR and Western blotting techniques. For additional details on primer sequences, antibodies, and shRNA, please refer to Tables S1 and S2, respectively.

Scratch Assays
Cells were seeded in 6-well plates during the logarithmic growth phase at a density of 1×10^5 cells per well. Subsequently, they were incubated in a 37°C, 5% CO_2 environment. When the cells reached around 90% confluence, scratch wounds were generated on the cell monolayer using a straight ruler. Afterward, the wells underwent three gentle washes with PBS to eliminate any detached cells, followed by the addition of serum-free medium. The cells were then returned to the same conditions for further incubation. Intermittent observations of cell migration were conducted using an inverted microscope. Images were captured at the beginning (0 hours) and end (24 hours) of the experiment to monitor migration progress, and closure rates were subsequently calculated to evaluate wound healing.

Transwell Migration Assays
For the Transwell migration assays, cells were seeded into the upper chamber at a density of 4×10^4 cells/300μL in serum-free culture medium. In the lower chamber, 500μL of culture medium supplemented with 20% fetal bovine serum was added. The chambers were then incubated at 37°C with 5% CO_2 for an additional 48 hours. Afterward, the cells were carefully removed, and the supernatant was aspirated. Fixation was performed with 4% paraformaldehyde for 20 minutes. After fixation, the upper chamber was gently wiped to eliminate non-migratory cells, and then rinsed with PBS. Following this, the insert was dried and examined under a microscope for documentation.

CCK-8 Viability Assays
The initial seeding density of cells in 96-well plates was 5×10^3 cells per well. After allowing the cells to adhere, they were treated with complete medium supplemented with 10% CCK-8 reagent. Following a 1-hour incubation period, the optical density at 490 nm was determined.

Assessment of tumor mutation burden (TMB) score, and cancer stem cell (CSC) index in high versus low-risk groups
To assess TMB score, and CSC index, we utilized various analytical approaches. We computed immune and stromal scores utilizing the ESTIMATE algorithm to compare components across both groups. Somatic mutations underwent analysis via the R package "maftools" with TMB documented for individual patients. Boxplots were utilized to evaluate the differential expression of immune checkpoints and their correlation with risk groups regarding CSC.

Drug Susceptibility Analysis

Therapeutic implications of the prognostic model in ACC were evaluated through drug susceptibility analysis. Using the R package "pRRophetic", IC50 values were calculated for various chemotherapeutic agents and targeted therapies commonly employed in clinical practice, across distinct risk groups. Statistical significance was determined accordingly.

Statistical Analysis

Statistical analyses were performed with R software (versions 4.1.3 and 4.2.0). Comparisons between two groups were conducted using Student's *t*-test or the Wilcoxon rank-sum test, while *ANOVA* was applied for comparisons involving multiple groups. A significance level of $p < 0.05$ was considered indicative of statistical significance.

Result

Exploring Cuproptosis Subtypes in ACC

Figure 1 presents the study's design concept. Survival data from TCGA and GEO were merged, excluding patients without survival information, resulting in a total of 123 patients included for comparison. RNA-seq data for 17 CRGs were obtained. Univariate Cox regression analysis was then performed to assess the prognostic significance of these 17 CRGs in ACC patients, as detailed in Table 1. Following this, a cuproptosis-associated prognostic network was constructed, illustrating the interactions among CRGs, their regulatory relationships, and their prognostic implications (Figure 2a). Among the 11 CRGs demonstrating significance in OS, LIAS, NLRP3, ATP7B, and PDHA1 were associated with longer OS, while SLC31A1, CDKN2A, FDX1, MTF1, NFE2L2, LIPT1, and DLAT were linked to shorter OS, as observed in Kaplan-Meier curves (Figure 2b–l).

We utilized a consensus clustering algorithm to examine the expression patterns of the 11 prognostic CRGs and classify cuproptosis in ACC. This analysis unveiled three distinct subtypes—referred to as subtypes A, B, and C (Figure 3a and Table S3)—comprising 48, 38, and 37 cases, respectively. Following PCA, notable distinctions in the
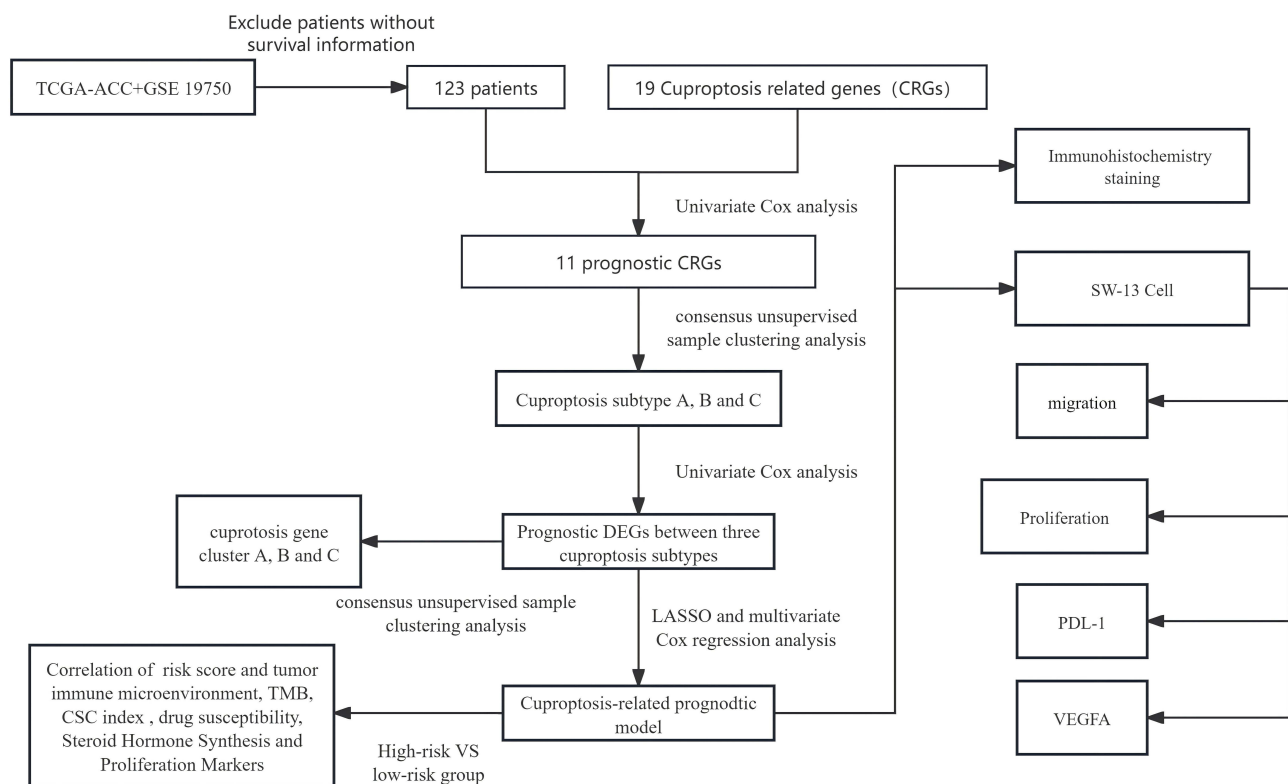

Figure 1 The flow chart of our study.

Table 1 Univariate Cox Regression Analysis of Cuproptosis Related Genes

Id	HR	HR.95L	HR.95H	P value	K-M
SLC31A1	2.131	1.559	2.913	<0.001	<0.001
CDKN2A	1.383	1.130	1.693	0.002	<0.001
FDX1	1.197	0.998	1.437	0.053	0.003
MTF1	1.885	1.112	3.197	0.019	0.004
NFE2L2	1.330	0.941	1.880	0.107	0.010
LIAS	0.736	0.495	1.093	0.129	0.011
NLRP3	0.669	0.345	1.298	0.235	0.018
ATP7B	0.979	0.392	2.447	0.964	0.021
PDHA1	0.773	0.539	1.108	0.160	0.025
LIPT1	1.441	0.875	2.373	0.151	0.026
DLAT	1.264	0.914	1.747	0.156	0.032
DLST	1.119	0.862	1.455	0.398	0.056
ATP7A	0.856	0.581	1.261	0.430	0.061
PDHB	1.176	0.800	1.729	0.409	0.071
GLS	0.874	0.660	1.157	0.347	0.084
DLD	0.968	0.733	1.279	0.820	0.134
DBT	0.964	0.594	1.567	0.884	0.283

transcriptional patterns of cuproptosis were illuminated among these subtypes (Figure 3b). Survival analysis unveiled significant prognostic differences within the three cuproptosis subtypes, with subtype C displaying remarkable survival benefits (Figure 3c). Additionally, supplementary investigations unveiled varying expressions of CRGs and clinical characteristics across the three subtypes (Figure 3d).

TME Characteristics and Functional Diversity in Cuproptosis Subtypes

For a deeper understanding of the variations in survival among the three subtypes, GSVA enrichment analysis was employed to reveal their unique functional and biological characteristics. By comparing the enrichment analysis results between subtypes A and C, B and C, as well as A and C, we uncovered noteworthy insights. Subtype B exhibited a pronounced association with pathways related to cell division and DNA repair, whereas subtype C showed significant enrichment in metabolic pathways, including linoleic acid metabolism (Figure 4a–c).

Moreover, we evaluated the enrichment levels of 23 distinct immune cell subpopulations across the three subtypes utilizing ssGSEA analysis (Figure 4d). Subtype C was distinguished by its significant infiltration of a wide array of immune cell types, including activated B cells, CD8 T cells, dendritic cells, natural killer cells, myeloid-derived suppressor cells (MDSCs), macrophages, monocytes, natural killer T cells, plasmacytoid dendritic cells, and type 17 T helper cells. In contrast, subtype B showed conspicuous infiltration of activated CD4 T cells and type 2 T helper cells, while subtype A exhibited the highest eosinophil infiltration.

Discovery of Gene Clusters Among DEGs

Utilizing the limma R package, we delved into the biological intricacies associated with each cuproptosis pattern, leading to the identification of 230 DEGs across the three clusters (Figure 5a). Subsequently, we conducted functional analysis focusing on these DEGs. GO analysis (Figure 5b) revealed significant enrichment of DEGs involved in biological processes related to cell proliferation, such as nuclear division, organelle fission, and chromosome segregation. The most enriched molecular function annotations included tubulin binding, microtubule binding, and histone binding. Additionally, KEGG pathway analysis highlighted the considerable engagement of the top 20 enriched pathways in cellular processes such as the cell cycle and DNA replication (Figure 5c).

Through univariate Cox regression analyses, we pinpointed 214 prognostic DEGs with significant associations to OS ($P < 0.05$, Table S4). Subsequently, we utilized the We performed a consistency analysis using the Consensus Cluster
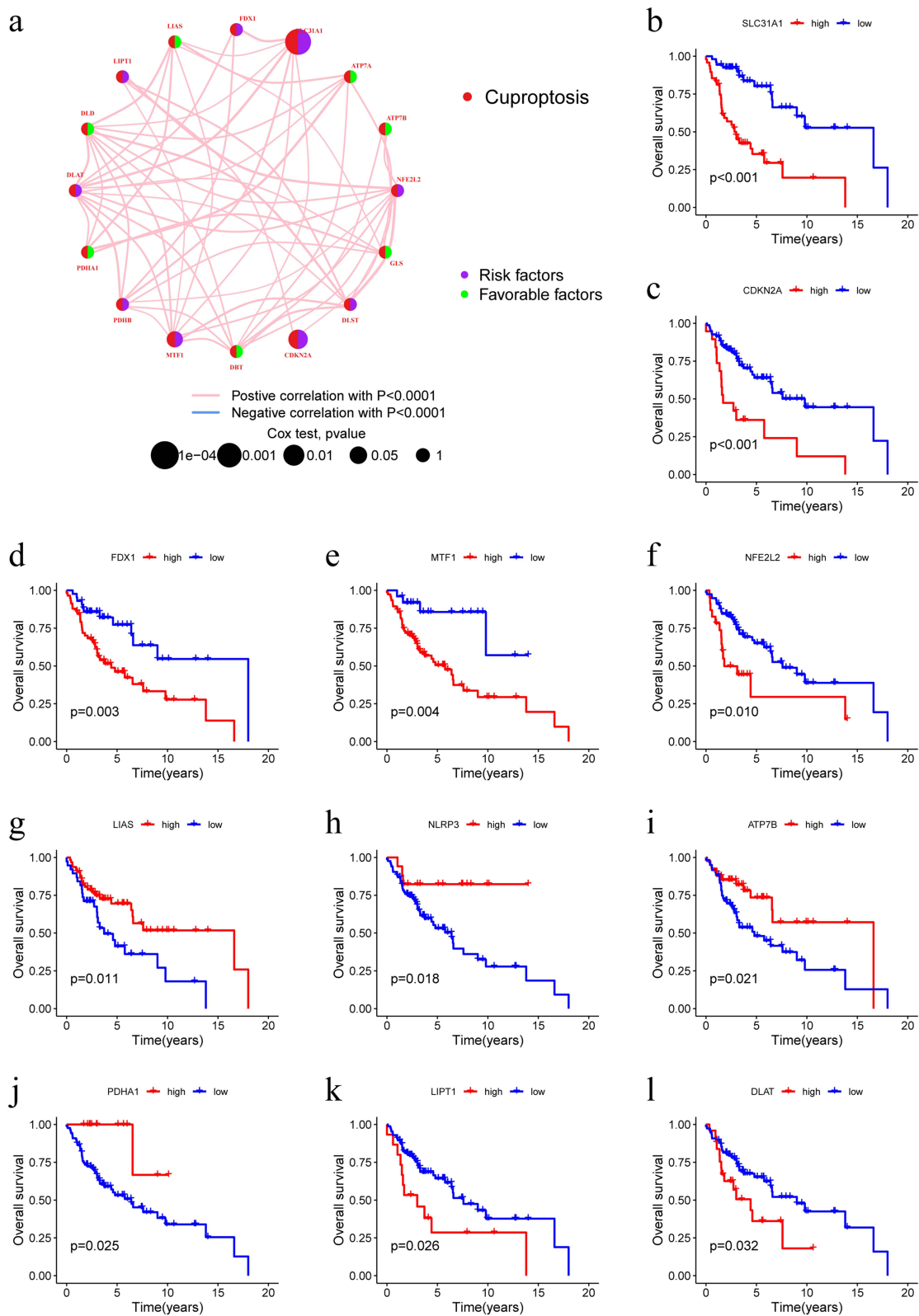
Figure 2 Interaction Network and Survival Analysis of CRGs in ACC. (**a**) Interactions among CRGs in ACC. The line connecting the CRGs represents their interaction. Blue represents negative and pink represents positive correlations. (**b–l**) Kaplan-Meier curves based on the expression of CRGs (SLC31A1, CDKN2A, FDX1, MTF1, NFE2L2, LIAS, NLRP3, ATP7B, PDHA1, LIPT1, and DLAT).
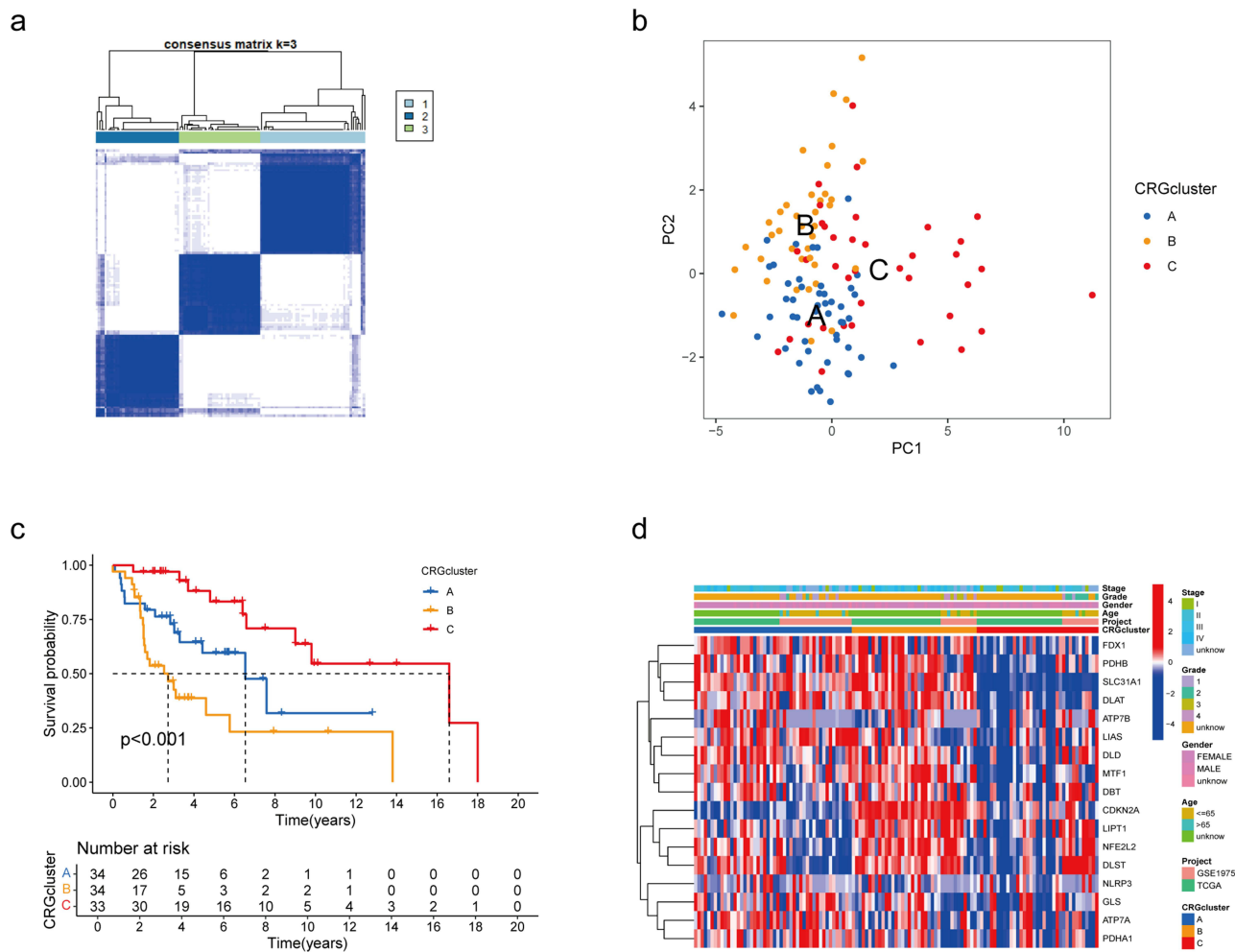
Figure 3 Cuproptosis subtypes in ACC. (**a**) Consensus matrix heatmap defining three subtypes (k = 3) and their correlation area. (**b**) PCA analysis showing a significant difference in cuproptosis in transcriptomes between the three subtypes. (**c**) Survival analysis showed significant differences among the three cuproptosis subtypes. (**d**) Differences in clinical features and CRGs expression between three cuproptosis subtypes.

Plus package in R software, dividing ACC patients into three cuproptosis gene clusters labeled as gene cluster A, gene cluster B, and gene cluster C (k = 3, Figure 5d and Table S5). Kaplan–Meier curves for survival analysis demonstrated a noteworthy discrepancy in OS among the three clusters, notably with cluster C exhibiting superior OS ($P < 0.001$) (Figure 5e). Additionally, Figure 5f delineates the relative disparities in stage, pathological grade, gender, age, and cuproptosis subtypes across gene clusters A, B, and C. Noteworthy differences were discerned in the expression profiles of the 17 CRGs across the three gene clusters, as depicted in Figure 5g.

Development and Validation of the Prognostic CRG_score

The datasets from TCGA and GEO pertaining to ACC were amalgamated and subsequently divided randomly into training and validation sets in a 1:1 ratio.LASSO analysis identified six genes, which were further analyzed using multivariate Cox regression to establish a risk signature (Figure 6a and b). As a result of this procedure, two prognostic CRGs were identified: ASF1B was identified as a high-risk gene, whereas NDRG4 was classified as a low-risk gene (Table 2). The CRG_score was computed using coefficients derived from the multivariate Cox regression analysis as follows: CRG risk score = (0.7043 * ASF1B expression) + (−0.3375 * NDRG4 expression). The stratification of patients into high-risk and low-risk groups was determined by using the median risk score as the threshold. Figure 6c illustrates the distribution of patients across cuproptosis subtypes, gene clusters, risk scores, and OS status. Figure 6d and e highlights a significant contrast in CRG_score among the cuproptosis subtypes and gene clusters, with subtype C demonstrating the lowest CRG_score,
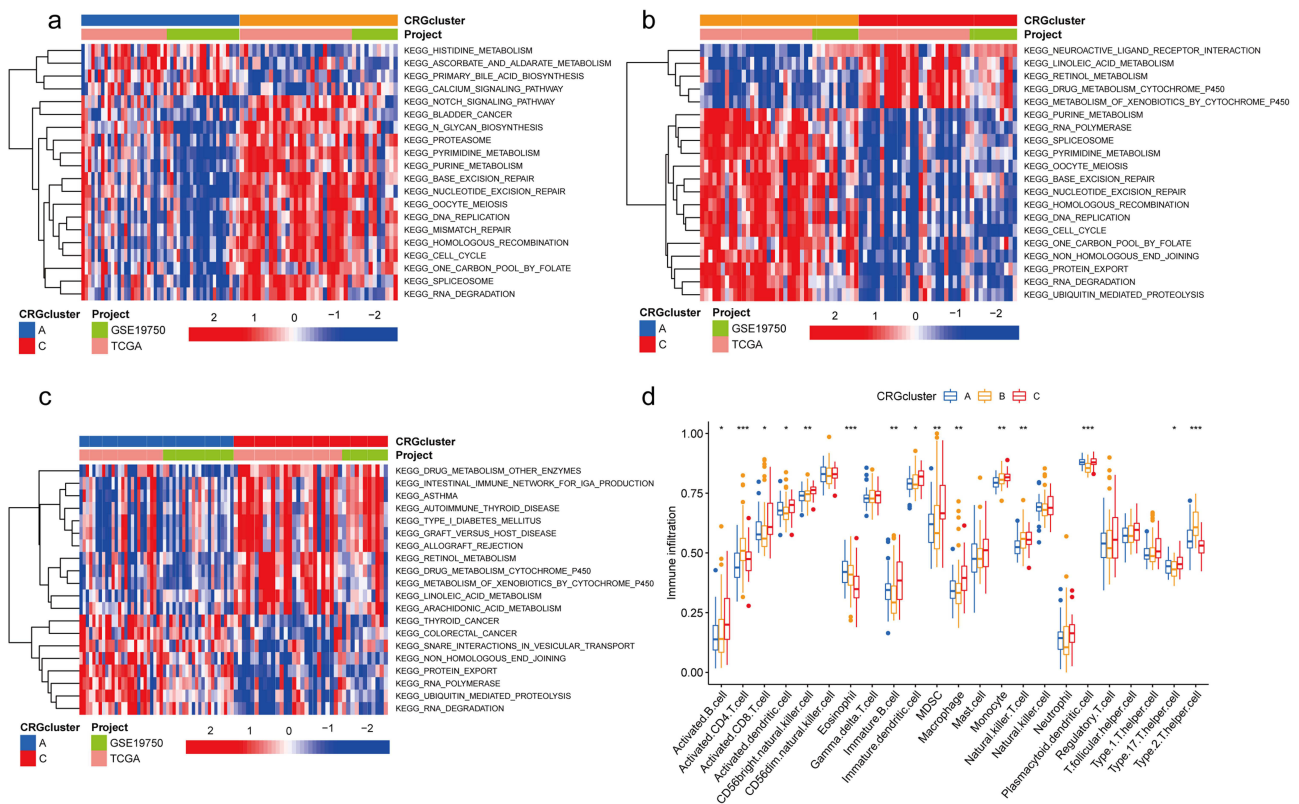
Figure 4 GSVA of Biological Pathways and Immune Cell Infiltration in Cuproptosis Subtypes. (**a–c**) GSVA of biological pathways between two distinct subtypes. (**d**) Abundance of 23 infiltrating immune cell types in the three cuproptosis subtypes. Statistical significance is indicated with *$P < 0.05$; **$P < 0.01$; ***$P < 0.001$.

and subtype B displaying the highest CRG_score. Furthermore, Figure 6f showcases significant differential expression of eight CRGs between the high-risk and low-risk groups.

In the training cohort, the distribution plot (Figure 6g) revealed a reduction in OS as the CRG_score increased. Kaplan–Meier survival analysis indicated significantly better OS in patients with low scores compared to those with high scores ($P < 0.001$; Figure 6h). Furthermore, the CRG_score displayed 1-, 3-, and 5-year survival rates with corresponding area under the curve (AUC) values of 0.979, 0.975, and 0.869, respectively (Figure 6i). A heatmap was also generated to visualize the relationships between the two prognostic marker genes and the CRG risk groups, revealing high expression of ASF1B in the high-risk group and elevated expression of NDRG4 in the low-risk group (Figure 6j). These trends were consistently observed across both the entire dataset and the validation set (Figure S1).

Assessment of Tumor Microenvironment in High- and Low-Risk Cohorts

Using the ESTIMATE algorithm, our analysis revealed that the high-risk group demonstrated significantly lower stromal score, immune score, and overall ESTIMATE Score compared to the low-risk group (Figure 7a, Table S6). This finding suggests a less favorable tumor microenvironment in the high-risk cohort, which could have implications for immune cell infiltration and the tumor's ability to evade immune surveillance.

Association of CRG_score with CSC Index, Mutation Status, and Drug Sensitivity

Analyzing somatic mutations across the patient cohort, we compared their distribution between the two CRG_score groups. Noteworthy among the top ten mutated genes were MUC16, CTNNB1, TP53, TTN, PCDH15, ASXL3, CNTNAP5, SVEP1, and LRP1. Significantly, the high-risk group exhibited a markedly higher mutation frequency compared to the low-risk group (88.89% vs 48.78%, Figure 7b and c). Furthermore, the high-risk cohort exhibited an elevated TMB (Figure 7d and e).
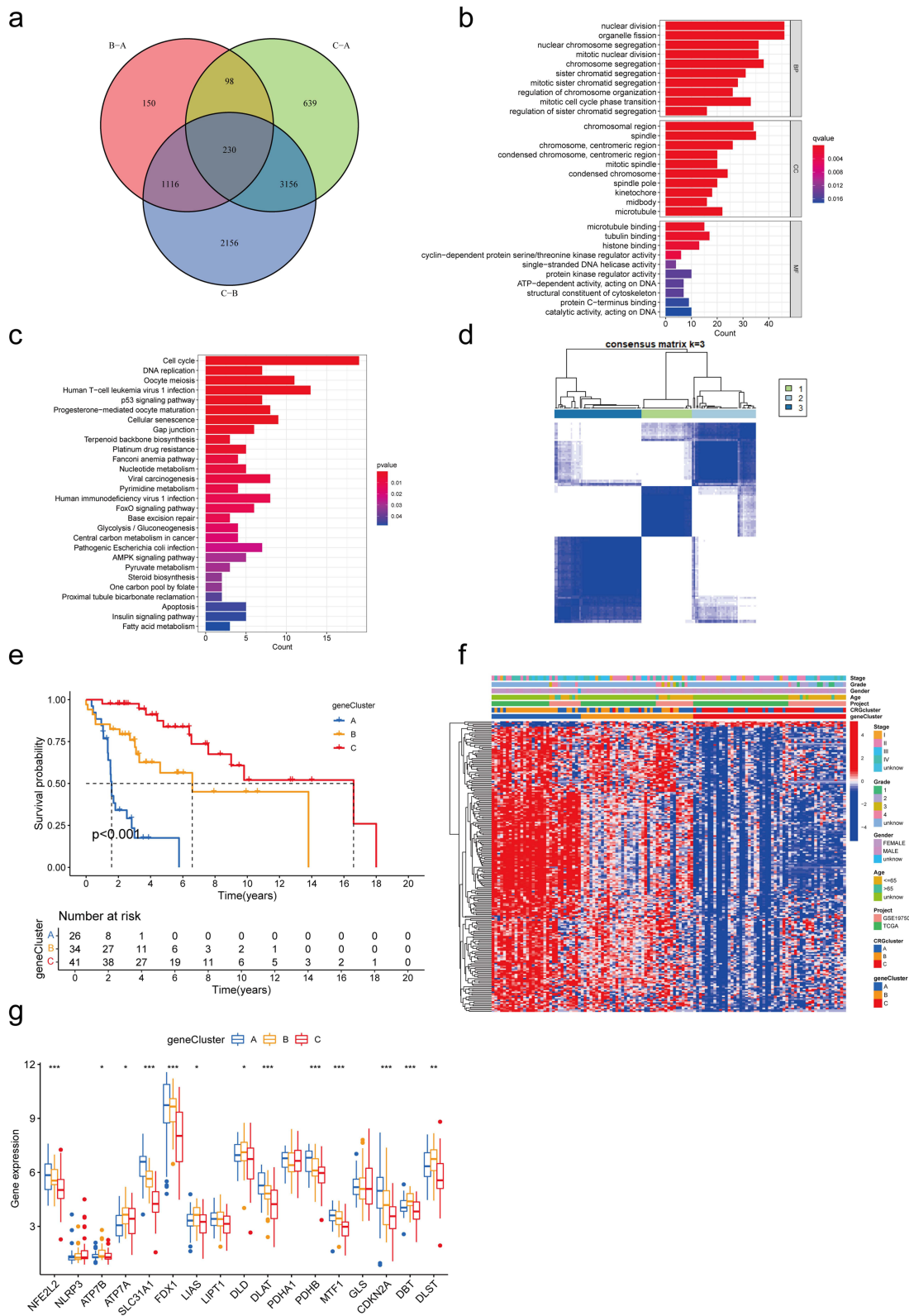
Figure 5 Identification of gene clusters based on DEGs. (**a**) The Veen diagram showed the intersection of DEGs based on the three cuproptosis subtypes. (**b** and **c**) GO and KEGG enrichment analyses of DEGs. (**d**) Consensus matrix heatmap defining three cuproptosis-related prognosis gene clusters (k = 3). (**e**) Survival analysis showed significant differences among the three prognosis gene clusters. (**f**) Differences in clinical features and CRGs expression among the three prognosis gene clusters. (**g**) Differences in the expression of 17 CRGs among the three prognosis gene clusters. Statistical significance is indicated with *P < 0.05; **P < 0.01; ***P < 0.001.
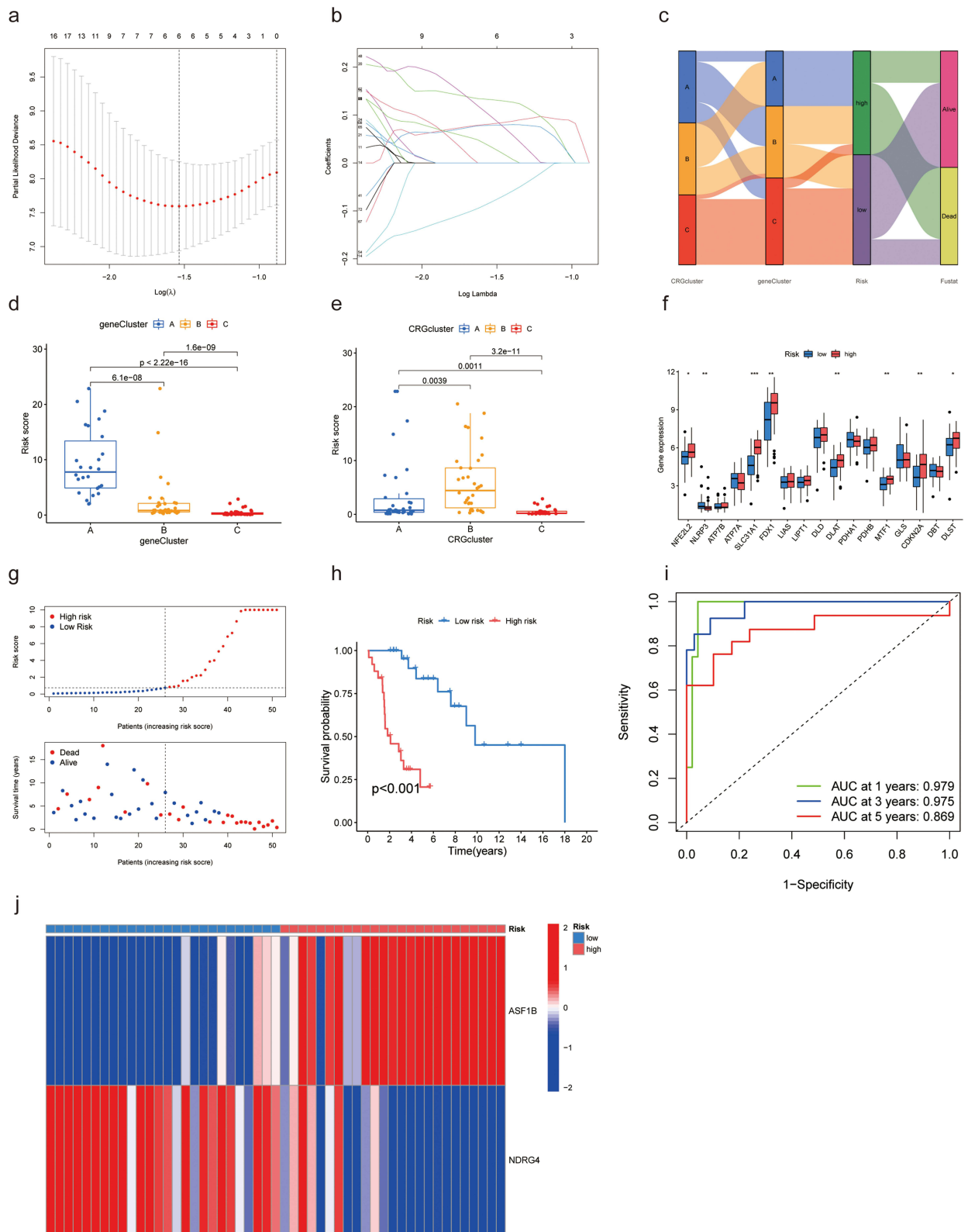
Figure 6 Development and Validation of Risk Signature for ACC Prognosis: (**a** and **b**) LASSO regression analysis and partial likelihood deviance of the prognostic genes. (**c**) Distribution of patients across cuproptosis subtypes, gene clusters, risk_score, and OS status. (**d**) Comparison of CRG_score among the three gene clusters. (**e**) Comparison of CRG_score among the three cuproptosis subtypes. (**f**) Differential expression of eight CRGs between high-risk and low-risk groups. (**g**) Distribution plot showing the association between CRG_score and OS in the training cohort. (**h**) Kaplan-Meier survival curves demonstrating significantly better OS in low-score patients compared to high-score patients. (**i**) AUC values representing the 1-, 3-, and 5-year survival rates based on CRG_score. (**j**) Heatmap illustrating the expression patterns of the two prognostic marker genes (ASF1B and NDRG4) in different CRG risk groups. Statistical significance is indicated with *$P < 0.05$; **$P < 0.01$; ***$P < 0.001$.

Table 2 Prognostic Genes in
the Risk Score

Id	Coef
ASF1B	0.7043
NDRG4	−0.3375

A notable finding was the significant positive linear correlation observed between the CRG_score and the CSC index (R = 0.54, p < 0.001). This suggests that ACC cells with higher CRG_scores tend to display increased stem cell properties and decreased differentiation levels (Figure 7f).

Regarding drug sensitivity, individuals in the high-risk category exhibited decreased IC50 values for Doxorubicin and Etoposide (Figure 7k–l). These observations highlight the potential of CRG_score as a predictive factor for drug sensitivity, aiding in the selection of appropriate treatment strategies for ACC patients.

Steroid Hormone Synthesis and Proliferation Markers in High-Risk Vs Low-Risk Groups

Jordan et al[14] compiled a list of genes involved in steroid metabolism, including those associated with cortisol synthesis and related transcription factors. A comparison of mRNA expression levels of steroid synthesis genes between the high-risk and low-risk groups revealed elevated expression of CYP17A1, HSD3B1, HSD3B2, HSD11B2, CYP19A1, PBX1, CREB1, and NR5A1 in the high-risk group, with lower NR0B1 expression (Figure 7g).

The correlation between the CRG_score and proliferation markers such as MKi67 and mitotic count was also assessed. The high-risk group exhibited higher expression of MKi67, with a positive correlation observed between CRG_score and MKi67 expression (Figure 7h and i). Additionally, a higher CRG_score was proportional to increased mitotic count (Figure 7j).

Validation of Protein Expression Levels of Risk Genes in ACC Tissue via IHC Staining

Significant alterations in the protein expression levels of ASF1B and NDRG4 were observed in ACC tissue compared to adrenocortical adenoma tissue, as indicated by IHC results. Specifically, ASF1B exhibited a notable upregulation in ACC tissue, whereas NDRG4 demonstrated a marked downregulation (Figure 8a-d) relative to their expression in adrenocortical adenoma tissue.

Divergent Roles of ASF1B and NDRG4 in Regulating Migration, Proliferation, Angiogenesis, and Immune Modulation in SW-13 Adrenocortical Carcinoma Cells

To investigate the functional significance of ASF1B and NDRG4 in ACC, we utilized specific shRNAs to downregulate their expression in SW-13 cells. We identified the two shRNAs with the highest knockdown efficiency for subsequent experiments through qRT-PCR and Western blot assays (Figure 9a–f). Following scratch and transwell experiments, it was observed that ASF1B knockdown attenuated SW-13 cell migration capacity, while NDRG4 knockdown enhanced migration (Figure 9g–i, k). Furthermore, CCK-8 assay results demonstrated that ASF1B suppression reduced SW-13 cell proliferation, while NDRG4 inhibition increased proliferation (Figure 9j). These findings highlight the pro-migratory and proliferative roles of ASF1B in SW-13 cells, contrasting with the inhibitory effects of NDRG4.

Additionally, we assessed the expression of PDL-1 and VEGFA following the knockdown of ASF1B and NDRG4. ASF1B knockdown was associated with an increase in PDL-1 expression and a decrease in VEGFA expression. In contrast, NDRG4 knockdown led to a decrease in PDL-1 expression and a significant increase in VEGFA expression (Figure 10).
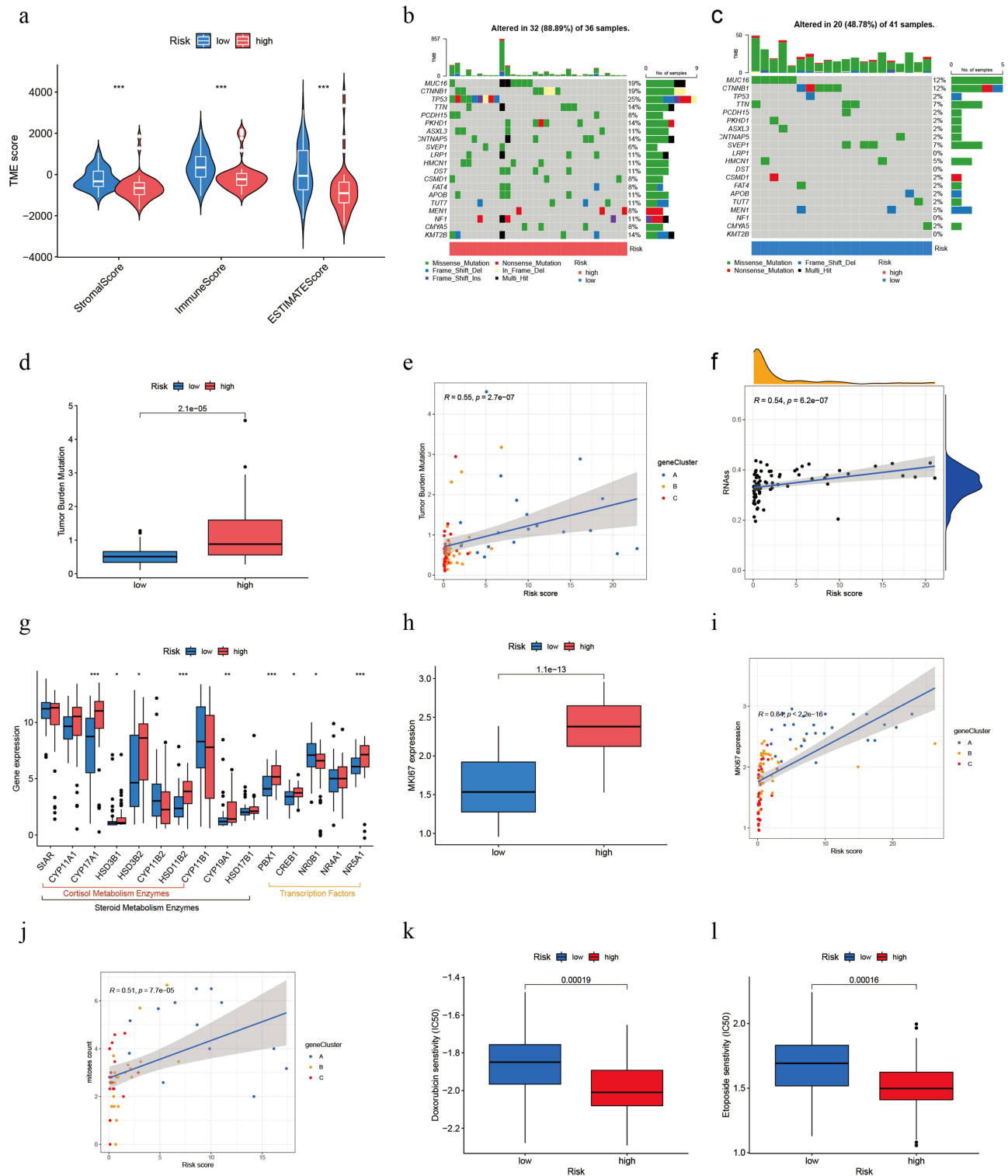
Figure 7 Analysis of Tumor Microenvironment, Mutation Status, Cancer Stem Cell Index, Drug Sensitivity, and Hormone Synthesis in High- and Low-Risk ACC Cohorts Based on CRG_score. (**a**) Comparison of Stromal Score, Immune Score, and ESTIMATE Score Between High-Risk and Low-Risk Groups. (**b** and **c**) Distribution and Frequency of Somatic Mutations in High-Risk and Low-Risk Groups. (**d**) TMB Analysis in High-Risk and Low-Risk Groups. (**e**) Correlation Between CRG_score and TMB, and Its association with Cuproptosis Gene Clusters. (**f**) Correlation Between CRG_score and CSC Index, and Its association with Cuproptosis Gene Clusters. (**g**) mRNA Expression Levels of Steroid Synthesis Genes in High-Risk and Low-Risk Groups. (**h**) MKi67 in High-Risk and Low-Risk Groups. (**i**) Correlation Between CRG_score and MKi67, and Its association with Cuproptosis Gene Clusters. (**j**) Association of CRG_score with Mitotic Count. (**k** and **l**) Drug Sensitivity Analysis for Doxorubicin and Etoposide in High-Risk and Low-Risk Groups. Statistical significance is indicated with *$P < 0.05$; **$P < 0.01$; ***$P < 0.001$.
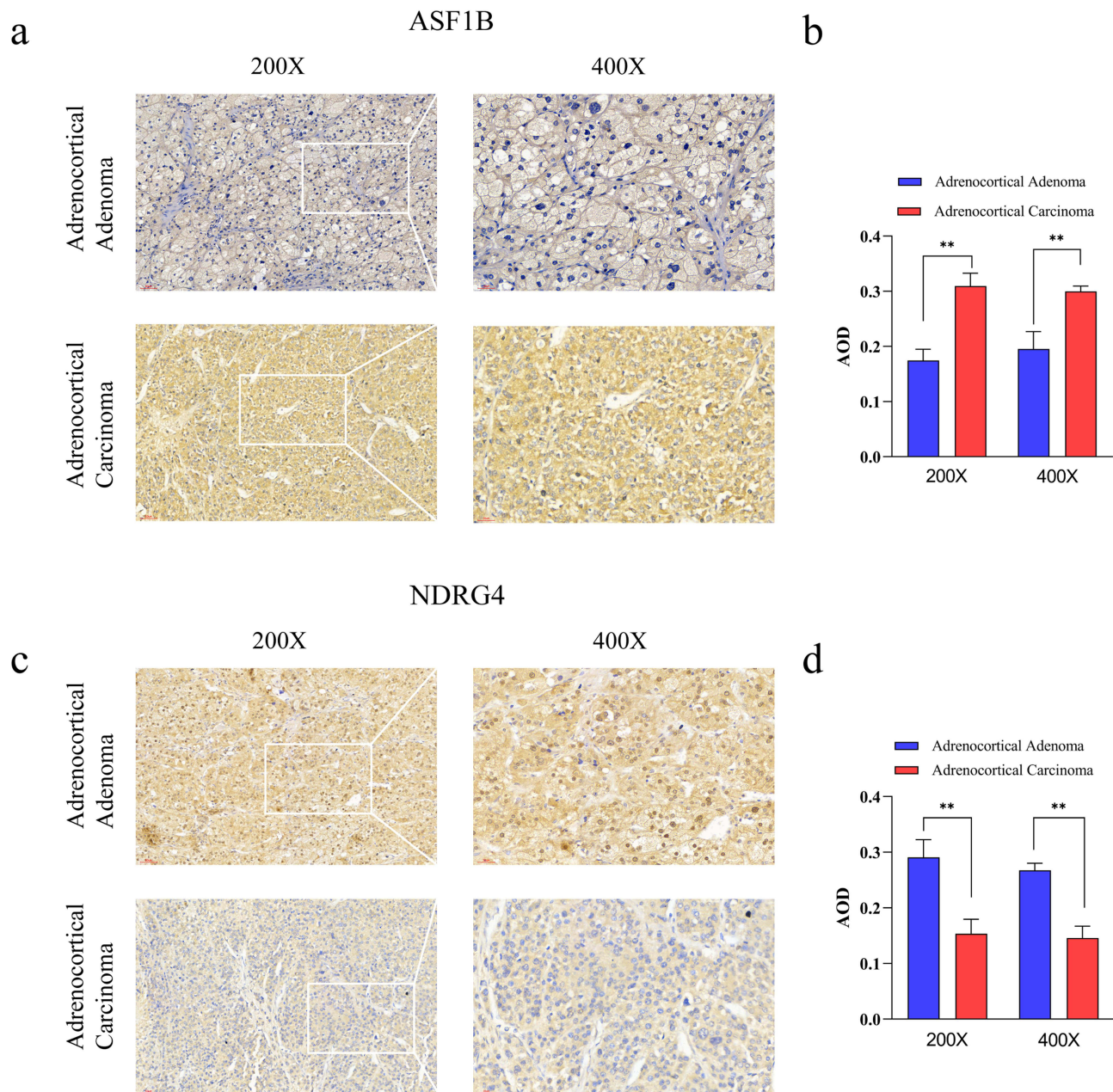
Figure 8 Protein Expression Levels of ASF1B and NDRG4 in ACC and adrenocortical adenoma Tissues. (**a** and **b**) Protein expression and semi-quantitative analysis of ASF1B. (**c** and **d**) Protein expression and semi-quantitative analysis of NDRG4. Statistical significance is indicated with *******P* < 0.01.

Discussion

Copper serves as a vital mineral nutrient essential for the functioning of all living organisms.[15] Disruptions in the precise equilibrium of copper ions have been linked to the onset and advancement of cancer.[16] Earlier studies have suggested a robust association between copper levels and the staging of breast and colorectal cancers.[17,18] Moreover, studies have underscored the role of copper in activating angiogenic factors like angiogenin and vascular endothelial growth factor, pivotal for tumor advancement and metastasis.[19] Cuproptosis, recognized as a new pathway of cell death, involves copper-triggered cell demise specifically targeting lipoylated TCA cycle proteins.[6] Research on cuproptosis in ACC remains limited. Further studies are needed to elucidate the mechanisms and potential clinical implications of cuproptosis in ACC.

Using the expression levels of 11 prognostic CRGs, we classified ACC patients into three distinct copper death-related subtypes (A, B, and C). Significant differences in OS were observed among these subtypes, with subtype
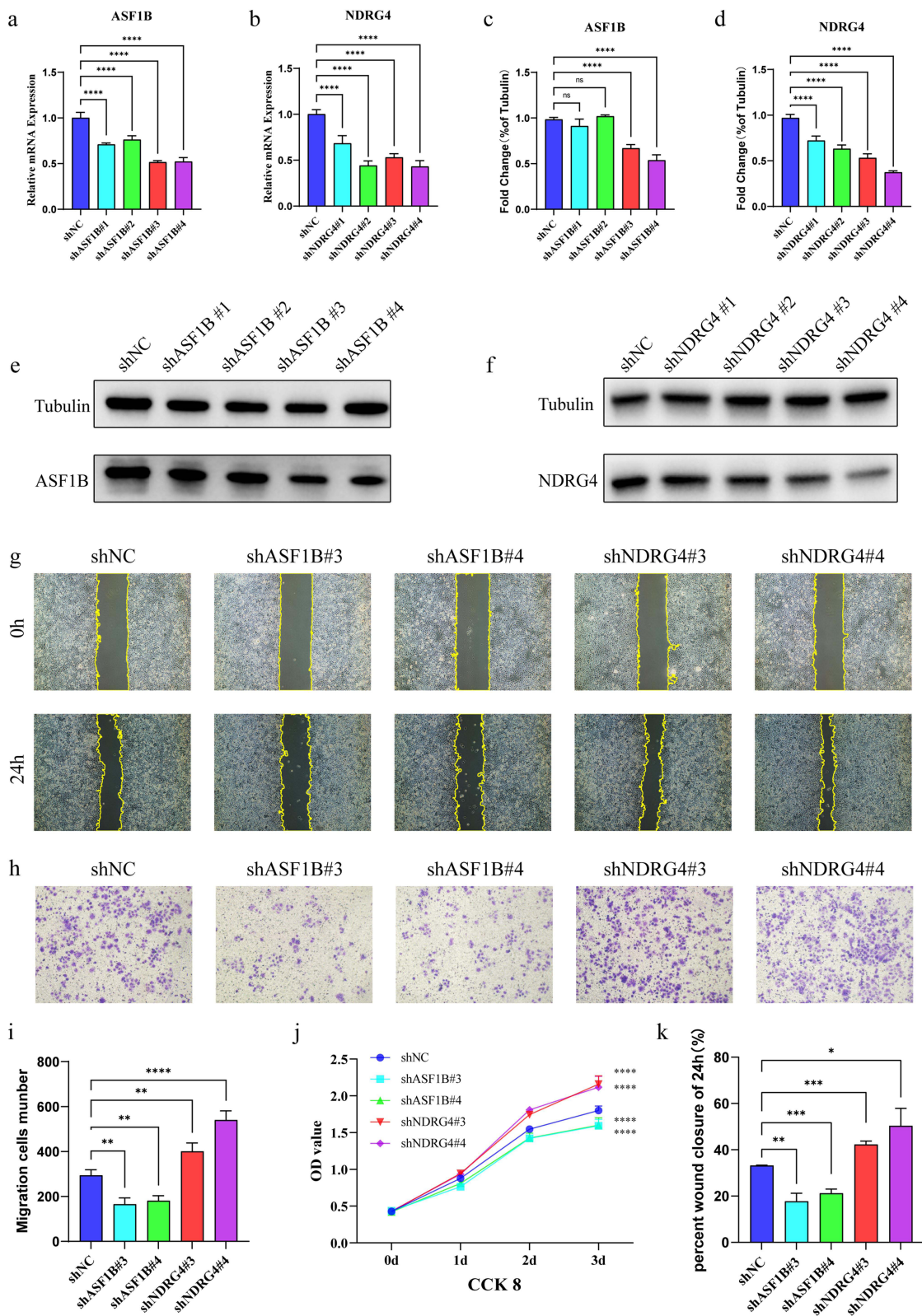
Figure 9 Functional Validation of ASF1B and NDRG4 Knockdown in SW-13 Cells. Validation of the interference efficiency of ASF1B and NDRG4 shRNAs in SW-13 cells through qRT-PCR (**a** and **b**) and Western blot (**c**–**f**). Scratch assay (**g** and **k**): Comparison of cell migration in different groups of SW-13 cells at 0h and 24h.Transwell migration assay (**h** and **i**): Evaluation of downward migration of SW-13 cells in different groups after 48h of seeding. CCK-8 assay (**j**): Relative cell proliferation rate-time curves of SW-13 cells in different groups. Statistical significance is indicated with *$P < 0.05$; **$P < 0.01$; ***$P < 0.001$; ****$P < 0.0001$; ns: not significant.
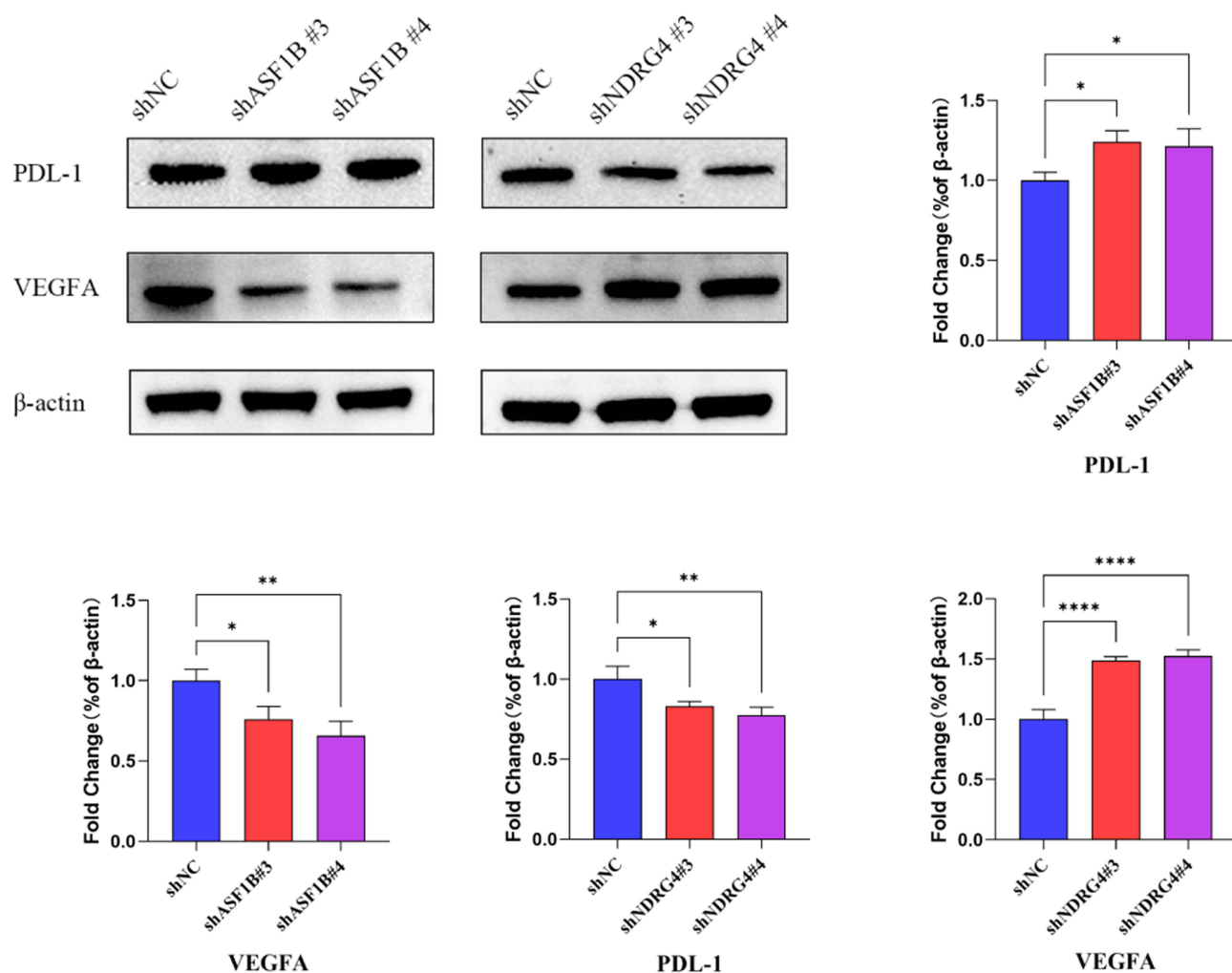
Figure 10 Effects of ASF1B and NDRG4 Knockdown on PDL-1 and VEGF-A Expression in SW-13 Cells. Statistical significance is indicated with *$P < 0.05$; **$P < 0.01$; ****$P < 0.0001$.

B exhibiting the poorest prognosis and subtype C the most favorable outcomes. Additionally, immune infiltration and functional characteristics varied markedly across the subtypes. Notably, no enrichment of tumor immune therapy-related pathways was identified in any of the three subtypes. We intersected the prognostic genes from all three subtypes and conducted univariate regression analysis, resulting in 214 cuproptosis DEGs. Functional enrichment analysis revealed that these DEGs were predominantly involved in cell proliferation pathways. Based on DEG expression, we further categorized patients into three gene clusters (A, B, and C), which also showed significant differences in OS. Most CRGs exhibited differential expression across these gene clusters. Building on these findings, we developed a prognostic model incorporating two cuproptosis DEGs, ASF1B and NDRG4.

ASF1B, a paralog of ASF1, plays a crucial role as a histone H3-H4 chaperone protein, governing processes such as DNA replication, repair of DNA damage, and regulation of transcription. Its main function involves facilitating cell proliferation and modulating cell cycle advancement.[20,21] Increasing evidence underscores ASF1B's significant involvement in the pathogenesis and prognosis of various cancers, such as lung adenocarcinoma,[20,22] hepatocellular carcinoma,[23] and gliomas.[24] Agosta et al[19] uncovered the role of NDRG4 in the miR-139-5p/NDRG4 axis, contributing to ACC aggressiveness and suggesting implications for prognosis and therapeutic strategies in adrenocortical malignancies. Additionally, Zhang et al[25] reported downregulation of NDRG4 protein and mRNA expression in gastric cancer, with significant associations noted with tumor differentiation, metastasis, stage, and unfavorable disease-free and OS.

Consistent with previous results, subtype B and cluster A demonstrated higher CRG_scores, while subtype C and cluster C had the lowest scores. Furthermore, patients in the high-risk group showed poorer prognosis. ROC curve analysis indicated that the CRG_score effectively predicted 1-, 3-, and 5-year survival rates, with time-dependent AUC values ranging from 0.673 to 0.979 at one year, 0.878 to 0.975 at three years, and 0.851 to 0.869 at five years across the three cohorts. In summary, we established a robust and effective prognostic CRG_score and validated its predictive performance.

Mitotic count and Ki67 are key prognostic markers for ACC. Previous research identified Ki67 as the most critical predictor of recurrence in localized ACC following R0 resection.[26] In our study, we observed that MKi67 was significantly elevated in the high-risk group, and both MKi67 expression and mitotic count were positively correlated with CRG_score. This correlation indicates that tumor cells in the high-risk group possess a higher proliferative capacity. Further, after knocking down the risk-associated genes, our findings were consistent with earlier results. Specifically, silencing the positive gene ASF1B led to reduced cell proliferation and migration, accompanied by decreased VEGFA expression. Conversely, knockdown of the negative gene NDRG4 resulted in increased cell proliferation and migration, along with elevated VEGFA expression. These results further confirm that tumors in the high-risk group are more aggressive and possess a greater capacity for angiogenesis.

ACC patients exhibit elevated steroid hormone secretion, primarily cortisol.[14] Studies suggest that increased hormone secretion in ACC is a significant risk factor for poor prognosis.[27] Glucocorticoids suppress the growth and maturation of immune cells, inhibit activation signals, and induce lymphocyte apoptosis.[28] Excessive glucocorticoids can impair immune function, thereby facilitating tumor progression.[14] We compared steroid secretion-related genes and transcription factors between high-risk and low-risk groups. The high-risk group showed increased expression of CYP17A1, HSD3B1, HSD3B2, HSD11B2, CYP19A1, PBX1, CREB1, and NR5A1, while NR0B1 expression was decreased. Notably, NR0B1 is recognized as an inhibitor of steroid hormone biosynthesis.[29] These results indicate that the high-risk group is characterized by elevated expression of genes involved in cortisol and steroid hormone synthesis. Overall, the high-risk group exhibits higher expression of genes promoting steroid hormone secretion, suggesting a higher level of steroids, which may contribute to resistance to immunotherapy. This finding partly explains the poor prognosis observed in the high-risk group. We also utilized the ESTIMATE algorithm to evaluate stromal and immune scores. It was found that the high-risk group had lower stromal and immune scores, along with higher tumor purity, aligning with the hypothesis that steroids suppress immune cell activity.

We observed that patients in the high-risk group had a higher tumor mutation burden. The three most frequently mutated genes in this group were MUC16, CTNNB1, and TP53. MUC16 and TP53 are among the most commonly mutated genes in human cancers. Mutations in MUC16 are associated with enhanced tumor cell proliferation and metastatic potential.[30] When TP53 is mutated, its tumor-suppressive function is altered, promoting carcinogenesis.[31] This aligns with our previous cellular findings. CTNNB1 encodes β-catenin, a crucial downstream component of the Wnt signaling pathway. Mutations in CTNNB1 have been linked to significant immune evasion and resistance to anti-PD-1 therapy in hepatocytes.[32] Additionally, knockdown experiments of low-risk genes ASF1B and NDRG4 revealed that silencing ASF1B increases PDL-1 expression, while silencing NDRG4 reduces PDL-1 expression, indirectly suggesting lower PDL-1 levels in the high-risk group and potential insensitivity to PD-1 blockade therapy. Based on these findings, we cautiously hypothesize that patients in the high-risk group may be less responsive to immunotherapy, with a tendency toward immune evasion and resistance to PD-1 inhibitors compared to those in the low-risk group.

ACC who are not candidates for complete surgical resection, existing research suggests avoiding routine adrenal surgery in cases of widespread metastasis. Instead, therapy should be personalized based on prognostic factors, favoring either mitotane alone or combined with etoposide, doxorubicin, and cisplatin.[33] Du et al[34] showed that linking doxorubicin with a specific metal-organic framework can intensify mitochondrial damage, inhibit Cu-ATPase, and increase cellular sensitivity to copper ions, while also inducing immunogenic cell death and reducing tumor metastasis. Similarly, Wang et al[35] developed a delivery system that incorporated doxorubicin, camptothecin and Cu2+, which induced cuproptosis and activated the immune response in triple-negative breast cancer cells. Our analysis of drug sensitivity revealed that patients classified as high-risk exhibited lower IC50 values for doxorubicin and etoposide, suggesting increased sensitivity to these agents. Further development of metal-based frameworks to enhance the targeting specificity of chemotherapeutic drugs, along with exploring the potential synergistic effects between chemotherapy and immunotherapy, could offer new avenues for treating advanced ACC.

Cuproptosis, a distinct mechanism of cell demise, is reliant on mitochondrial respiration. This unconventional pathway offers potential for innovative therapeutic strategies in cancer treatment. This study has several significant limitations. First, our analysis primarily relies on retrospective data from public databases, without validation from our own patient cohort. Furthermore, our functional studies did not explore the interactions between immune cells and adrenocortical carcinoma (ACC) cells, nor did we associate specific cell lines with ACC subtypes. The limited number of patient samples available also prevented us from assessing the correlation between Weiss scores, Ki-67 labeling index, and ASF1B and NDRG4 expression within our cohort. Although we hypothesized a link between our findings and tumor immunotherapy, we did not investigate the relationship between ASF1B and NDRG4 immunoreactivity and factors such as tumor-infiltrating lymphocytes, PD-L1 status, or vascularity in our ACC cases. These findings warrant confirmation through large-scale prospective studies and additional in vivo and in vitro experiments.

Conclusions

This study explores the role of CRGs in ACC and identifies distinct subtypes based on copper-related gene expression. Our prognostic model, incorporating ASF1B and NDRG4, provides insights into patient risk stratification, with high-risk patients showing poorer outcomes and potential resistance to immunotherapy. The study's retrospective design and limited clinical data underscore the need for further research to validate and expand upon these results. Overall, this research offers a foundation for developing targeted therapies and improving treatment approaches for ACC.

Abbreviations

ACC, Adrenocortical carcinoma; Cu, Copper; CNVs, copy number variations; CRG, cuproptosis related gene; DEGs, differentially expressed genes; TIME, tumor immune microenvironment; CDF, cumulative distribution function; PCA, Principal Component Analysis; GSVA, Gene Set Variation Analysis; OS, overall survival; shRNAs, short hairpin RNAs; TMB, tumor mutation burden; CSC, cancer stem cell.

Ethics Declaration

This retrospective study was approved by The First Affiliated Hospital of Fujian Medical University's ethics committee and conducted in accordance with the principles of the Helsinki Declaration. Informed consent was obtained from all participants.

Author Contributions

All authors made a significant contribution to the work reported, whether that is in the conception, study design, execution, acquisition of data, analysis and interpretation, or in all these areas; took part in drafting, revising or critically reviewing the article; gave final approval of the version to be published; have agreed on the journal to which the article has been submitted; and agree to be accountable for all aspects of the work.

Funding

Disclosure

The authors report no conflicts of interest in this work.

References

1. Mizdrak M, Tičinović Kurir T, Božić J. The Role of Biomarkers in Adrenocortical Carcinoma: a Review of Current Evidence and Future Perspectives. *Biomedicines*. 2021;9(2):174. doi:10.3390/biomedicines9020174
2. Lerario AM, Mohan DR, Hammer GD. Update on Biology and Genomics of Adrenocortical Carcinomas: rationale for Emerging Therapies. *Endocr Rev*. 2022;43(6):1051–1073.

3. Glenn JA, Else T, Hughes DT, et al. Longitudinal patterns of recurrence in patients with adrenocortical carcinoma. *Surgery*. 2019;165(1):186–195. doi:10.1016/j.surg.2018.04.068

4. Tapiero H, Townsend DM, Tew KD. Trace elements in human physiology and pathology. *Copper Biomed Pharmacoth*. 2003;57(9):386–398. doi:10.1016/S0753-3322(03)00012-X

5. Lutsenko S. Copper trafficking to the secretory pathway. *Metallomics*. 2016;8(9):840–852. doi:10.1039/C6MT00176A

6. Tsvetkov P, Coy S, Petrova B, et al. Copper induces cell death by targeting lipoylated TCA cycle proteins. *Science*. 2022;375(6586):1254–1261. doi:10.1126/science.abf0529

7. Yang L, Zhang Y, Wang Y, Jiang P, Liu F, Feng N. Ferredoxin 1 is a cuproptosis-key gene responsible for tumor immunity and drug sensitivity: a pan-cancer analysis. *Front Pharmacol*. 2022;13:938134. doi:10.3389/fphar.2022.938134

8. Dong J, Wang X, Xu C, et al. Inhibiting NLRP3 inflammasome activation prevents copper-induced neuropathology in a murine model of Wilson's disease. *Cell Death Dis*. 2021;12(1):87. doi:10.1038/s41419-021-03397-1

9. Ren X, Li Y, Zhou Y, et al. Overcoming the compensatory elevation of NRF2 renders hepatocellular carcinoma cells more vulnerable to disulfiram/copper-induced ferroptosis. *Redox Biol*. 2021;46:102122. doi:10.1016/j.redox.2021.102122

10. Kong L, Deng J, Zhou X, et al. Sitagliptin activates the p62–Keap1–Nrf2 signalling pathway to alleviate oxidative stress and excessive autophagy in severe acute pancreatitis-related acute lung injury. *Cell Death Dis*. 2021;12(10):928. doi:10.1038/s41419-021-04227-0

11. Leibovitz A, McCombs WM, Johnston D, McCoy CE, Stinson JC. New human cancer cell culture lines. I. SW-13, small-cell carcinoma of the adrenal cortex. *J Natl Cancer Inst*. 1973;51(2):691–697.

12. Avena P, De Luca A, Chimento A, et al. Estrogen Related Receptor Alpha (ERRα) a Bridge between Metabolism and Adrenocortical Cancer Progression. *Cancers*. 2022;14(16):3885. doi:10.3390/cancers14163885

13. Nocito MC, Avena P, Zavaglia L, et al. Adrenocortical Carcinoma (ACC) Cells Rewire Their Metabolism to Overcome Curcumin Antitumoral Effects Opening a Window of Opportunity to Improve Treatment. *Cancers*. 2023;15(4):1050. doi:10.3390/cancers15041050

14. Baechle JJ, Hanna DN, Sekhar KR, Rathmell JC, Rathmell WK, Baregamian N. Integrative computational immunogenomic profiling of cortisol-secreting adrenocortical carcinoma. *J Cellular Molecular Medi*. 2021;25(21):10061–10072. doi:10.1111/jcmm.16936

15. Ruiz LM, Libedinsky A, Elorza AA. Role of Copper on Mitochondrial Function and Metabolism. *Front Mol Biosci*. 2021;8:711227. doi:10.3389/fmolb.2021.711227

16. Oliveri V. Selective Targeting of Cancer Cells by Copper Ionophores: an Overview. *Front Mol Biosci*. 2022;9:841814. doi:10.3389/fmolb.2022.841814

17. Sharma K, Mittal DK, Kesarwani RC, Kamboj VP, Null C. Diagnostic and prognostic significance of serum and tissue trace elements in breast malignancy. *Indian J Med Sci*. 1994;48(10):227–232.

18. Gupta SK, Shukla VK, Vaidya MP, Roy SK, Gupta S. Serum and tissue trace elements in colorectal cancer. *J Surg Oncol*. 1993;52(3):172–175. doi:10.1002/jso.2930520311

19. Lelièvre P, Sancey L, Coll JL, Deniaud A, Busser B. The Multifaceted Roles of Copper in Cancer: a Trace Metal Element with Dysregulated Metabolism, but Also a Target or a Bullet for Therapy. *Cancers*. 2020;12(12):3594. doi:10.3390/cancers12123594

20. Zhang W, Gao Z, Guan M, Liu N, Meng F, Wang G. ASF1B Promotes Oncogenesis in Lung Adenocarcinoma and Other Cancer Types. *Front Oncol*. 2021;11:731547. doi:10.3389/fonc.2021.731547

21. Peng H, Nogueira ML, Vogel JL, Kristie TM. Transcriptional coactivator HCF-1 couples the histone chaperone Asf1b to HSV-1 DNA replication components. *Proc Natl Acad Sci U S A*. 2010;107(6):2461–2466. doi:10.1073/pnas.0911128107

22. Feng Z, Zhang J, Zheng Y, Wang Q, Min X, Tian T. Elevated expression of ASF1B correlates with poor prognosis in human lung adenocarcinoma. *Per Med*. 2021;18(2):115–127. doi:10.2217/pme-2020-0112

23. Ouyang X, Lv L, Zhao Y, et al. ASF1B Serves as a Potential Therapeutic Target by Influencing Cell Cycle and Proliferation in Hepatocellular Carcinoma. *Front Oncol*. 2021;11:801506. doi:10.3389/fonc.2021.801506

24. Zhu H, Ouyang H, Pan X, et al. Increased ASF1B Expression Correlates With Poor Prognosis in Patients With Gliomas. *Front Oncol*. 2022;12:912101. doi:10.3389/fonc.2022.912101

25. Zhang Z, She J, Yang J, et al. NDRG4 in gastric cancer determines tumor cell proliferation and clinical outcome. *Mol Carcinog*. 2018;57(6):762–771. doi:10.1002/mc.22798

26. Libé R. Adrenocortical carcinoma (ACC): diagnosis, prognosis, and treatment. *Front Cell Dev Biol*. 2015;3:45. doi:10.3389/fcell.2015.00045

27. Puglisi S, Perotti P, Pia A, Reimondo G, Terzolo M. Adrenocortical Carcinoma with Hypercortisolism. *Endocrinol Metab Clin North Am*. 2018;47(2):395–407. doi:10.1016/j.ecl.2018.02.003

28. Quatrini L, Ricci B, Ciancaglini C, Tumino N, Moretta L. Regulation of the Immune System Development by Glucocorticoids and Sex Hormones. *Front Immunol*. 2021;12:672853. doi:10.3389/fimmu.2021.672853

29. Guzzetti C, Bizzarri C, Pisaneschi E, et al. Next-Generation Sequencing Identifies Different Genetic Defects in 2 Patients with Primary Adrenal Insufficiency and Gonadotropin-Independent Precocious Puberty. *Horm Res Paediatr*. 2018;90(3):203–211. doi:10.1159/000492496

30. Thomas D, Sagar S, Liu X, et al. Isoforms of MUC16 activate oncogenic signaling through EGF receptors to enhance the progression of pancreatic cancer. *Mol Ther*. 2021;29(4):1557–1571. doi:10.1016/j.ymthe.2020.12.029

31. Periyasamy M, Singh AK, Gemma C, et al. p53 controls expression of the DNA deaminase APOBEC3B to limit its potential mutagenic activity in cancer cells. *Nucleic Acids Res*. 2017;45(19):11056–11069. doi:10.1093/nar/gkx721

32. Zhu GQ, Wang Y, Wang B, et al. Targeting HNRNPM Inhibits Cancer Stemness and Enhances Antitumor Immunity in Wnt-activated Hepatocellular Carcinoma. *Cell Mol Gastroenterol Hepatol*. 2022;13(5):1413–1447. doi:10.1016/j.jcmgh.2022.02.006

33. Fassnacht M, Dekkers O, Else T, et al. European Society of Endocrinology Clinical Practice Guidelines on the management of adrenocortical carcinoma in adults, in collaboration with the European Network for the Study of Adrenal Tumors. *Eur J Endocrinol*. 2018;179(4):G1–G46. doi:10.1530/EJE-18-0608

34. Du C, Guo X, Qiu X, et al. Self-Reinforced Bimetallic Mito-Jammer for Ca2+ Overload-Mediated Cascade Mitochondrial Damage for Cancer Cuproptosis Sensitization. *Adv Sci*. 2024;11(15):e2306031. doi:10.1002/advs.202306031

35. Wang N, Liu Y, Peng D, et al. Copper-Based Composites Nanoparticles Improve Triple-Negative Breast Cancer Treatment with Induction of Apoptosis-Cuproptosis and Immune Activation. *Adv Healthc Mater*. 2024;12:e2401646. doi:10.1002/adhm.202401646